Supplementary material B: Petrography and mineral chemistry

In this supplementary text, we compile all thin section scans, microphotos and scanning electron microscope (SEM) results that could not be included in the paper due to space constraints. This, for a more primitive damtjernite dyke with both a porphyritic core and almost aphyric margins (519768M & -C in Fig. B1), two autolithic nodules inside 519714 (Fig. B4), a carbonaceous alnöite dyke sample 519749 (Fig. B6) and a phonolite nephelinite cone sheet sample 519711 (Fig. B8). In addition, raw SEM elemental maps, used to construct traced phase maps in the main paper's Figures 4(f-g), 5, 6(b) and 7(c-d), are compiled in Figures B2, B3, B5 and B7, respectively.

B1. Porphyritic damtjernite dykes with almost aphyric margins

Two sets of dyke samples were collected from almost aphyric margins and porphyritic centres of two thicker damtjernite dykes and their petrographies are compiled in Figures B1(e-h), B2 and B3, where the latter two supplement Figures 4 and 5, respectively. In Figure B1, the more primitive dyke (519768M & -C) from study area C (Fig. 2e) only has olivine, augite and magnetite phenocrysts, where olivines – unlike the other more evolved dyke – are not resorbed. Biotites are arguably restricted to the matrix, even if some biotite crystals are moderately sized. Modal proportions, derived from thin section scans in Figure B1(e-f), clearly show how much more porphyritic this dyke's core is, compared to its margin (47 *vs* 3 modal % phenocrysts, respectively, for 519768M & -C in Table B1). With regards to modal phenocryst proportions (out of 100%), the dyke margin sample (519768M) contains a greater proportion of magnetite micro-phenocrysts (22%) than its core (519768C), while a reverse relationship exists for olivine, which is almost absent (2%) in the margin and constitutes >¼ of all phenocrysts in the core. Only augite phenocrysts are more evenly distributed across this dyke, comprising roughly ¾ in both populations.

Table B1: Modal (micro-)phenocryst proportions (%) in traced images of damtjernite samples

Phase/Sample	519750A	519750B	519751	519768M	519768C
matrix	99	73	58	97	53
ocelli		1	6		
olivine		6	6	2	27
augite	62	55	53	76	72
magnetite	35	9	8	22	1
kaersutite/biotite	3	30	33		

Phenocryst proportions (out of 100%) exclude matrix and ocelli.

While phenocryst sizes for each of the above three phenocryst phases typically conform to negative exponential distributions, recognized as straight lines in logarithmic frequency *versus* spherical radius diagrams (Fig. B1g-h), their slopes – quantified by an inverse of their exponential coefficient (IEC = average of such distributions) – differ, but where there are expected increases for all three going from the dyke margin and into the core. While the dyke core's augite phenocrysts have little over twice as large radii, however, magnetite phenocrysts are three times larger and olivine phenocrysts almost six times larger, compared to phenocrysts within the dyke margin sample.

Figure B1 (following page): Petrography of 3.3 m-thick damtjernite dyke (519768M & -C). (a-b) Thin section scans of the chilled margin and porphyritic centre, where SEM spot analyses (cf., Fig. B9) are localized by colour-coded circles in (b). Red rectangles locate microphotos in (c-d), which contain (micro)phenocryst of olivine (ol), augite (au) and magnetite (mt); albeit, significantly larger in the core (d). Thin section scans of chilled margin (e) and porphyritic centre (f), with SEM spot locations colour coded as indicated by four phases. (g-h) Negative exponential size distributions are based on areas of traced (micro-)phenocrysts and ocelli in (e-f), where spherical radii = √area/π; i.e., from dyke margin to core (left-right) of more differentiated and northerly located dyke (top row a-c) and more primitive and southerly located dyke (bottom row d-e). Colour-coded numbers quantifies the inverse negative exponential coefficient (IEC) for the best fit through each population, intersecting x-axis at a population's maximum radius.

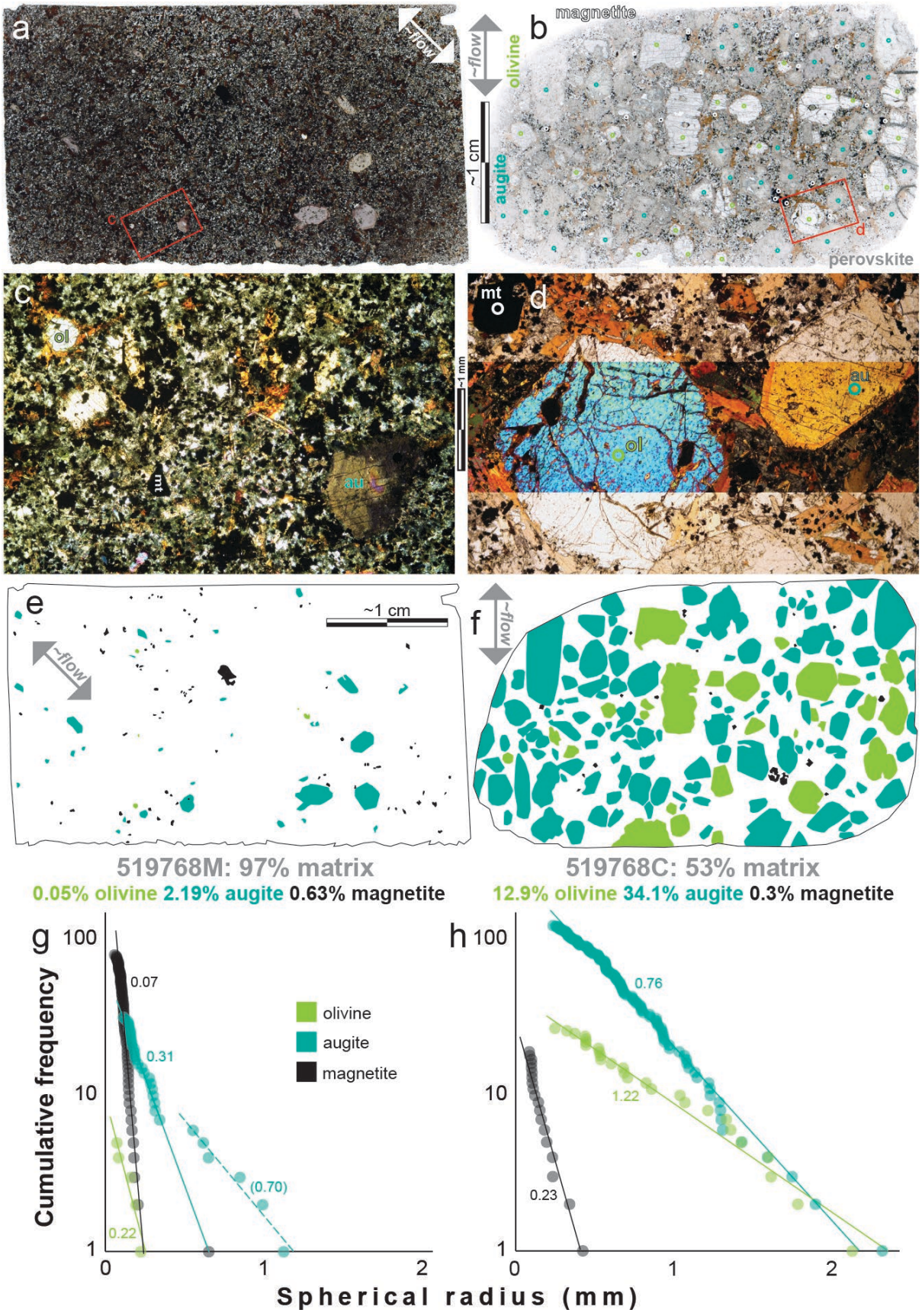

For the more evolved dyke, presented in the main paper, Figure B2 supplements Figure 4 with traced thin sections and size distributions for a more diverse population of phenocrysts, including additional kaersutite and biotite, as well as ocelli. While this dyke's margin sample 519750A (Fig. B2a) – like

the previous more primitive dyke – has a much larger proportion of magnetites, compared to the core, the margin does not host any olivine or ocelli.

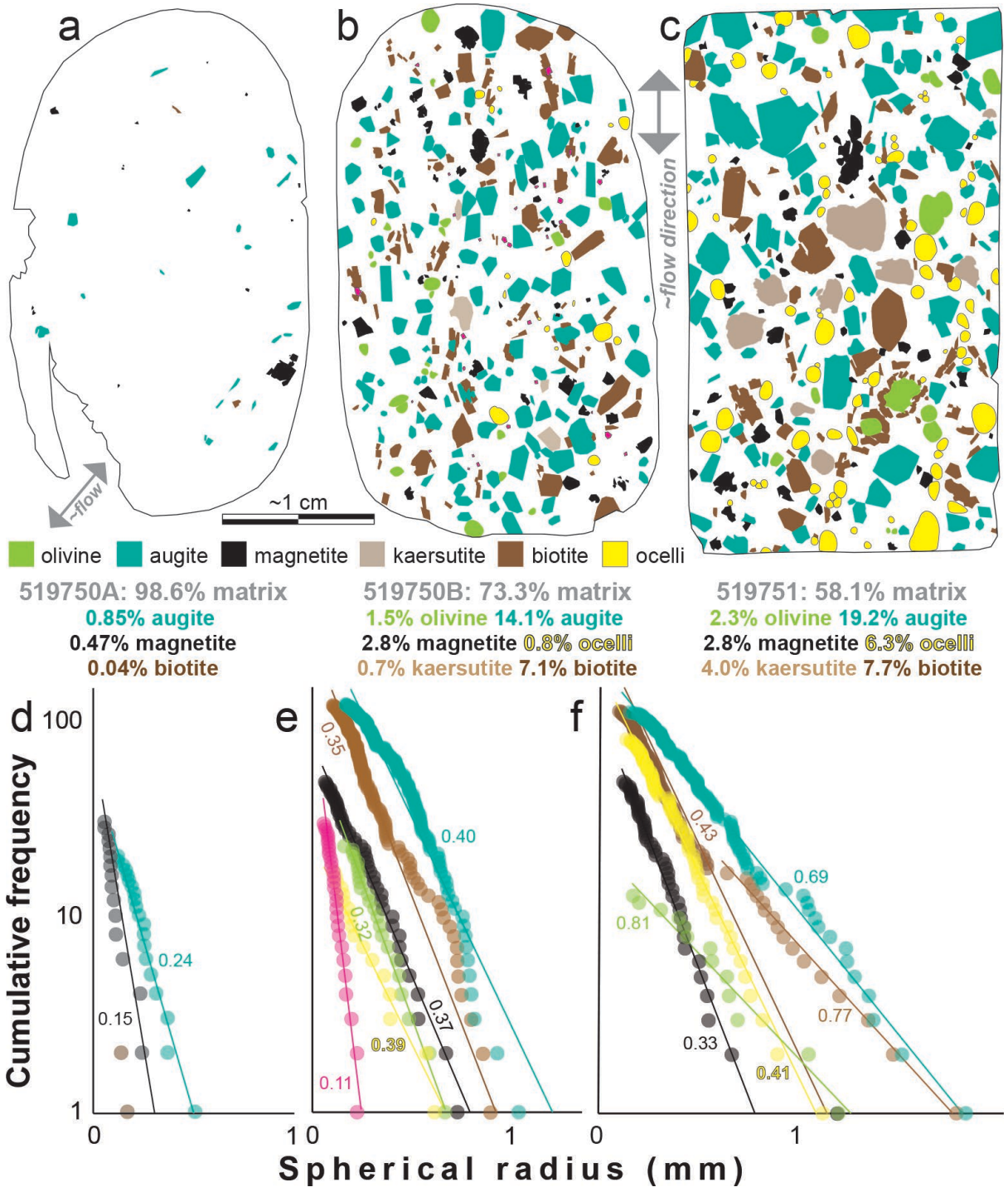

Figure B2: (Micro-)phenocrysts and ocelli within the most northerly dyke (Fig. 4d), traced from Figure 6(a-c) and colour-coded according to legend, but where some biotites/olivines in (b) may be kaersutite/serpentinized, respectively. (d-f) Negative exponential phenocryst and ocelli size distributions, as in Figure B1.

There is little difference between this more evolved dyke's two core samples (Fig. B2b-c & e-f), collected 156 m apart within study area N, other than all phenocrysts, except magnetites and ocelli, being consistently larger in the more northerly located core sample 519751. Within the presumed more marginal core sample 519750B (Fig. B2b), negative exponential size distributions of all ocelli and phenocrysts are parallel sloping (Fig. B2e), with IEC-values restricted between 0.32-0.40 mm.

For most silicate phenocrysts, size distribution slopes shallow inside the coarser core sample 519751, as reflected by increased IEC-values to between 0.69-0.81 mm. Only a smaller (<0.6 mm) fraction of the combined kaersutite and biotite distribution, together with magnetites and ocelli, roughly maintain their IEC-values (0.33-0.43). Magnetite micro-phenocrysts are overall smaller than those in the more evolved dyke, while both its augite and euhedral olivine phenocrysts are larger.

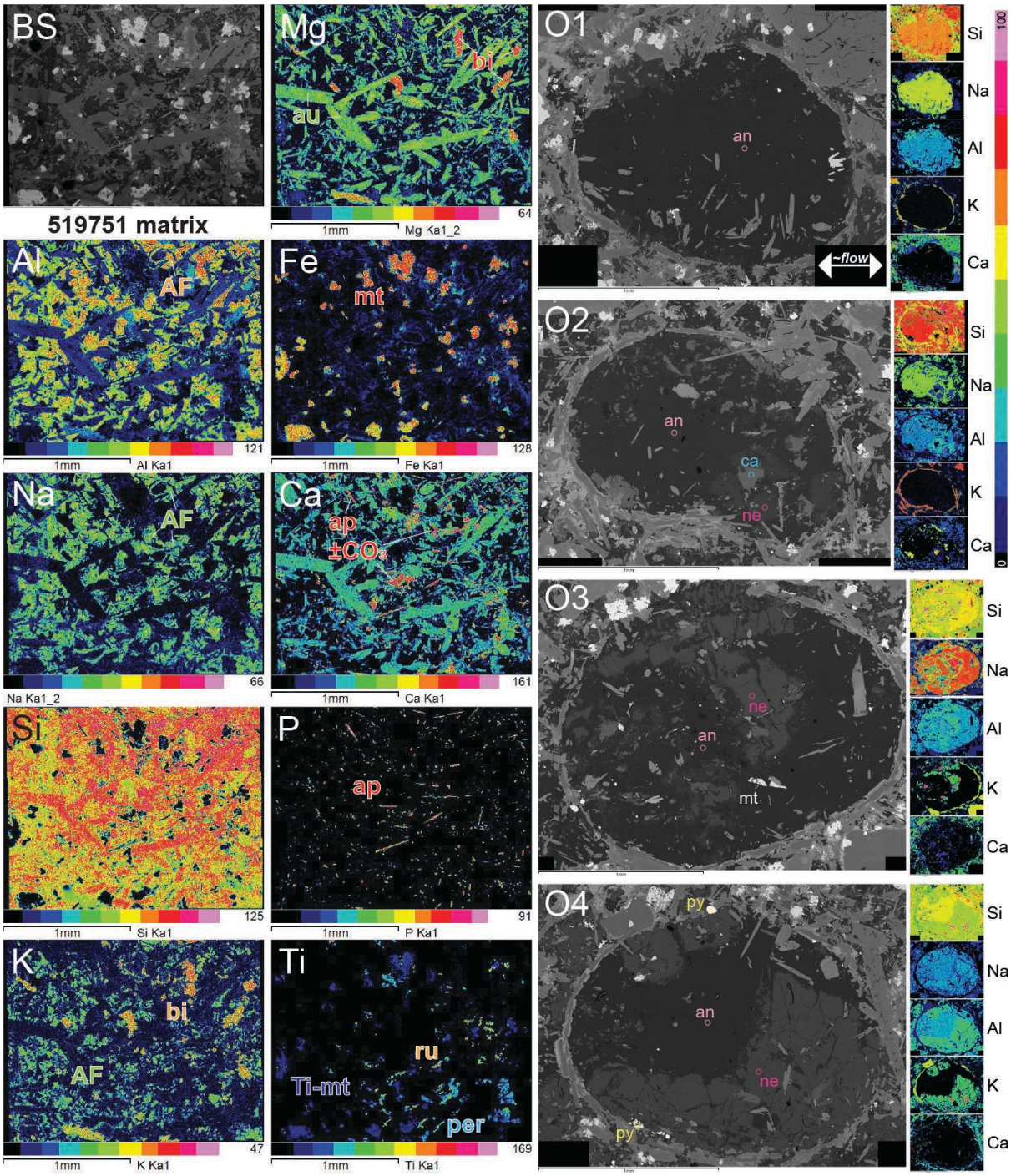

Figure B3: Raw SEM-imagery behind final phase maps for both matrix and four ocelli (Figs. 4f-g & 5a-d, respectively) inside sample 519751. (Left half) One grey-scaled electron backscatter and nine SEM element maps of matrix in Figure 4(c), with high-(Mg, Ca & Si) augites (au), high-(Al, Na & Si) alkali feldspars (AF), high-Fe magnetites (mt), high-Ca carbonates (CO_3), high-(P & Ca) apatites (ap), high-K biotites (bi) and high-Ti rutiles (ru), perovskites (per) & Ti-magnetites (Ti-mt). (Right half) Grey-scaled electron backscatter images of four ocelli (O1-4) inside 517751 (cf., Fig. 5). Five essential SEM element maps are shown for each, where colour scales roughly reflect relative concentration differences.

'Melt' proportions, represented by both matrix and ocelli, monitors the degree of accumulation (± flow segregation) of phenocrysts, even if ocelli may have segregated more easily towards dyke centres, due to both lower densities and relatively large sizes. Figure B3, provides SEM elemental maps and electron backscatter images of both the studied matrix and four ocelli within sample 519751, which supplement Figure s 4(d-g) and 5, respectively.

B2. Autolithic nodules in damtjernite sample 519714

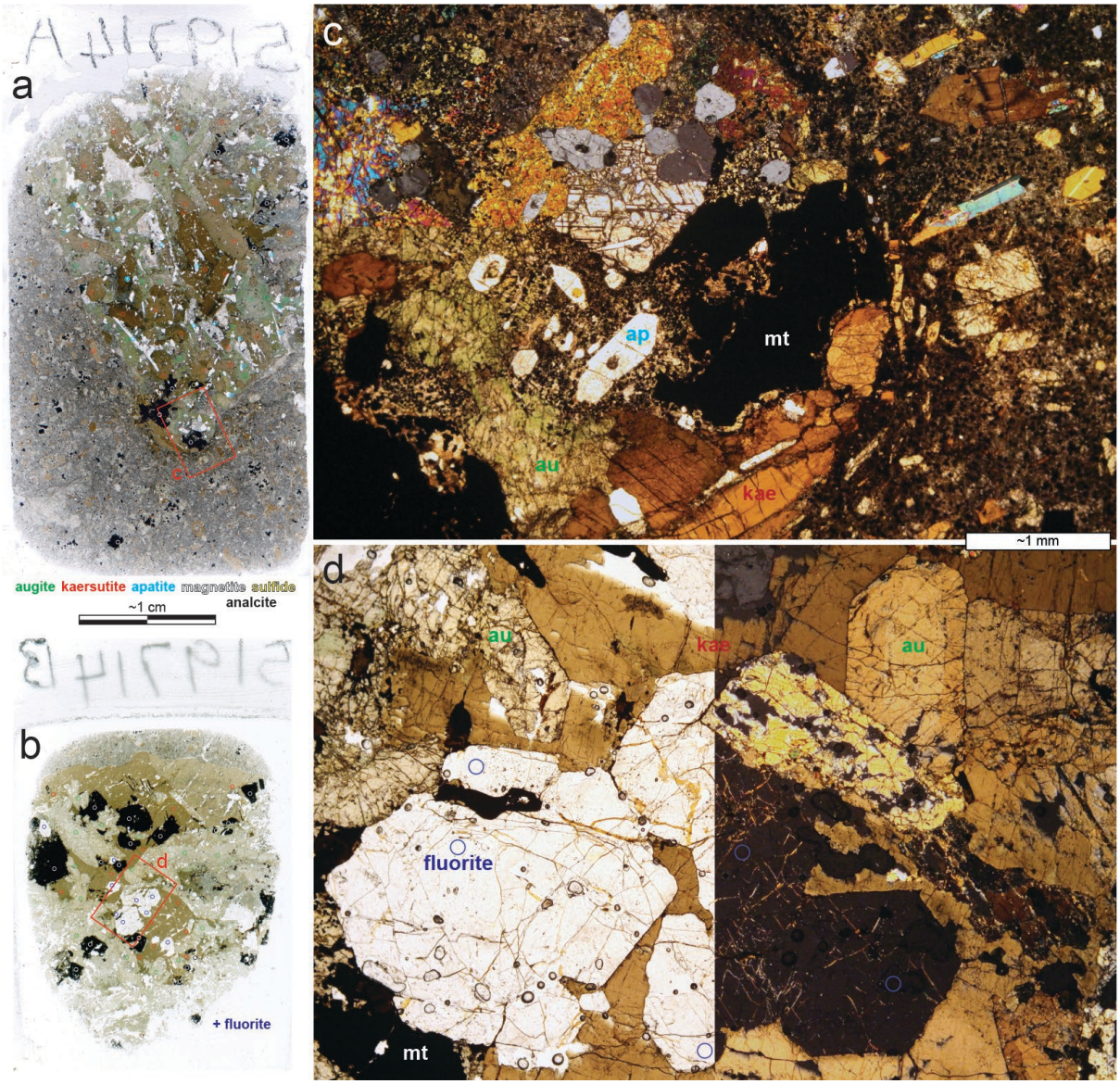

Figure B4: Two nodules inside a LMD dyke. (a-b) Thin section scan of 519714A & -B, respectively, including colour-coded circles that locate SEM spot analyses. (c) Microphoto of 519714A, showing cumulus augite (au) and apatite (ap), subhedral magnetite (mt) and more intercumulus kaersutite (kae), (d) Microphoto of 519714B, showing additional cumulus fluorite.

A thin section was made of each of two small nodules inside a LMD dyke sample 519714 (Fig. B4a-b), collected in study area S, most proximal to the aeromagnetic anomaly of the presumed carbonatitic centre to the FHI complex (Fig. 3e). Both nodules comprise of more euhedral augites, surrounded by subhedral magnetites and anhedral kaersitites. However, one nodule (Fig. B4a) also contains large proportions of euhedral apatites (Fig. B4c), while the other thin section (Fig. B4b) reveals euhedral and isotropic fluorites (Fig. B4d), not observed in any other FHI sample. The nodules likely represent cumulates from the magmatic centre that this dyke projects from and are thereby autoliths.

B3. Carbonaceous alnöites

Thin sections were made of two alnöite samples (519749 in Fig. B5 and 519754 in Figs. B6 & 6), which were both collected from study area N, most distal from FHI's carbonatitic centre (Fig. 3e). While the resolution of sample 519749's SEM elemental maps was too poor to resolve all its phases (Fig. B5b), this was not the case for sample 519754 in Figure 6(b), for which only supplementing SEM elemental maps and an electronic backscatter image are shown in Figure B6.

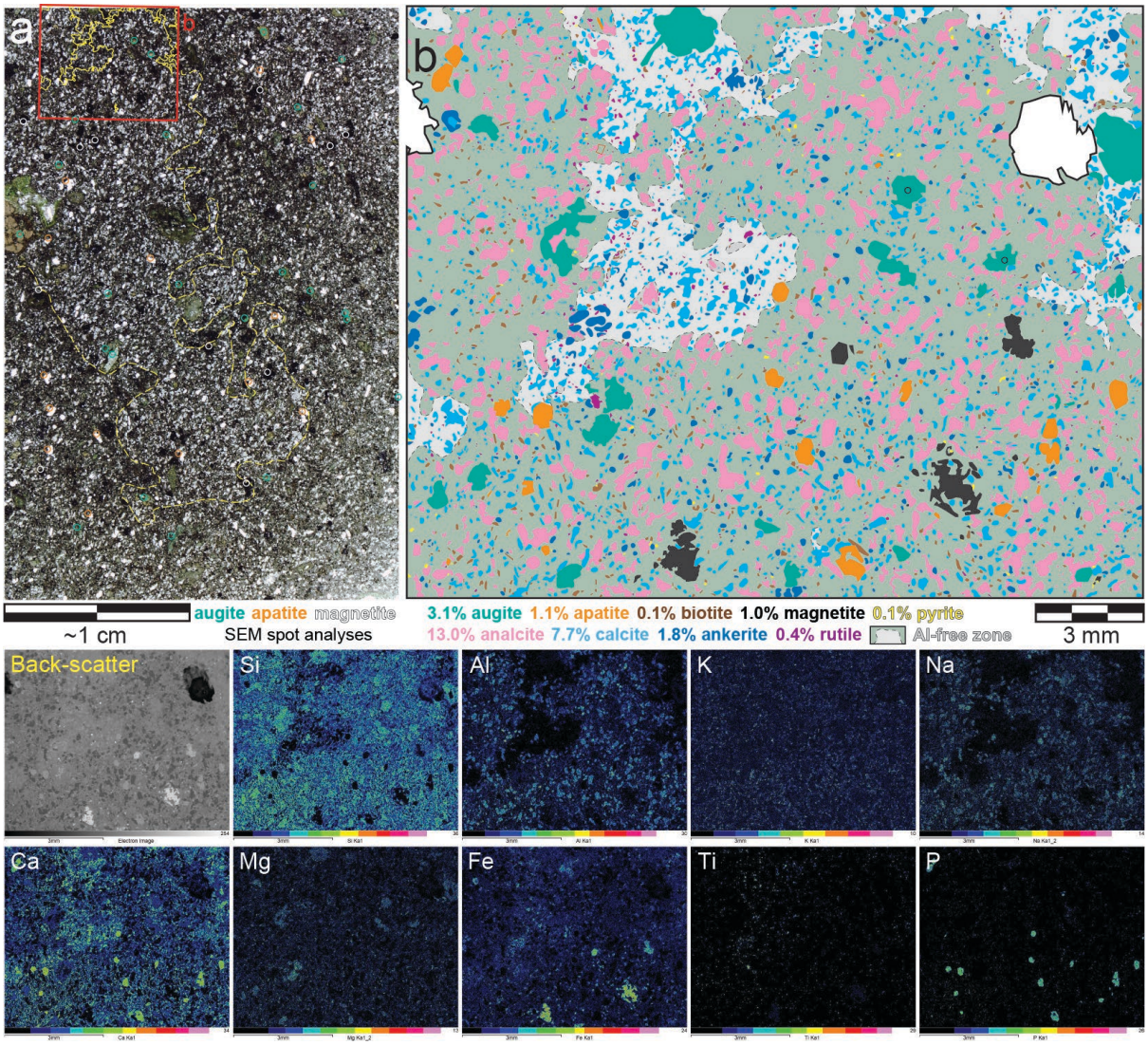

Figure B5: Deselected carbonaceous alnöite sample 519749. (a) Thin section scan, where colour-coded circles locate SEM spot analyses. (b) Incomplete 45.6 mm^2-large phase map of area located in (a), based on lowermost SEM electronic backscatter and nine element maps.

In the thin section scan for sample 519749 (Fig. B5a), one may discern a very faint and irregular zonation between slightly paler large patches (partly outlined by yellow line), surrounded by smaller intervening darker areas. SEM mapping (lower two rows in Fig. B5) reveals that paler parts are dominated by more aluminous phases, including analcime, and host most augites, magnetites, biotites and apatites, while darker areas are devoid of aluminium (cf., Al-map in Fig. B5) and contain a greater abundance of both calcite and ankerite, as well as rutile and rare augite micro-phenocrysts that likely crystallized before the phase segregation (Fig. B5b). For sample 519754, an electronic backscatter image and SEM elemental maps in Figure B6 supplement the phase map in Figure 6(b).

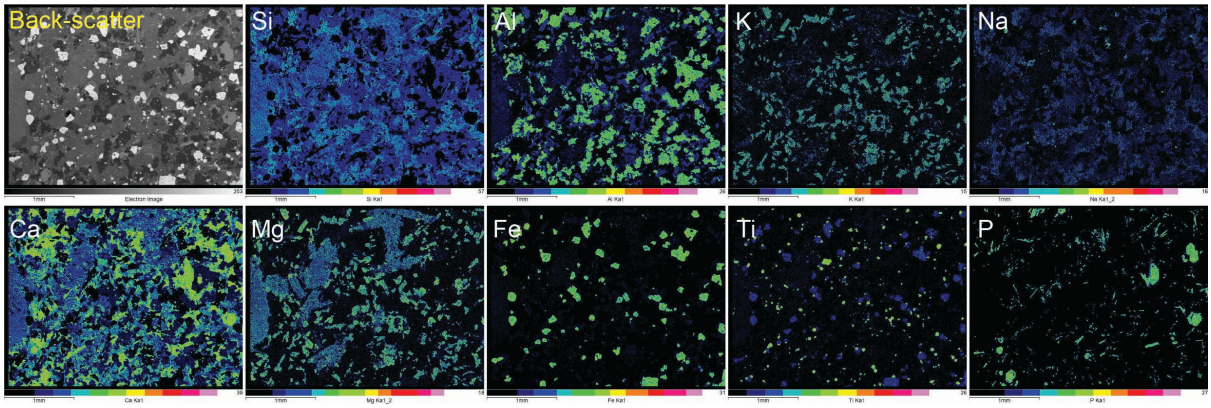

Figure B6: SEM back-scatter and nine elemental maps of matrix selection inside thin section of 519754 (cf., Fig. 6).

B4. Phonolitic nephelinites

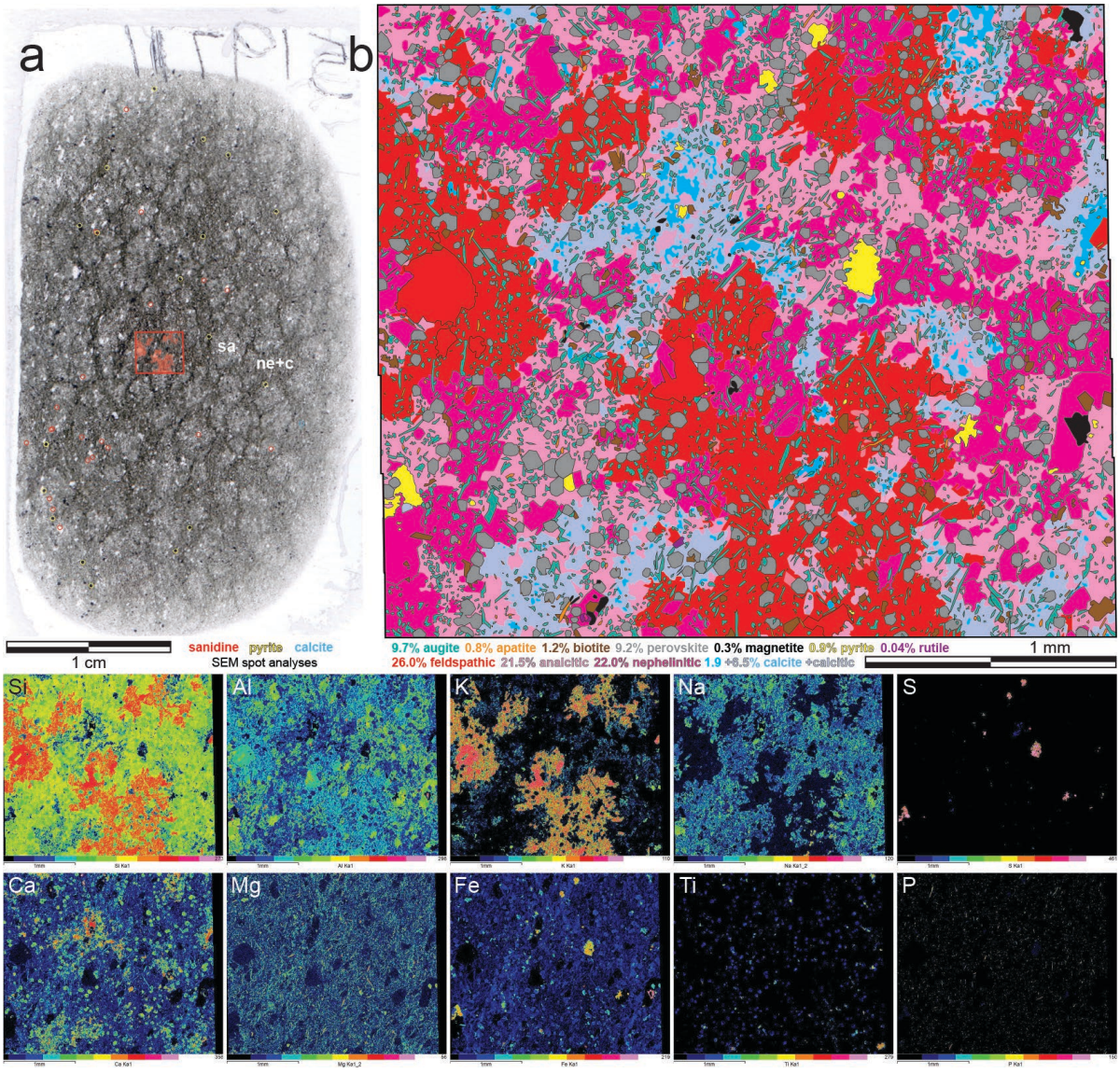

Figure B7: Deselected phonolitic nephelinite sheet sample 519711. (a) Thin section scan, where colour-coded circles locate SEM spot analyses. (b) Phase map of area located in (a), based on lowermost ten element maps.

A thin section was made from cone sheet sample 519711 (Fig. B7) and radiating dyke sample 519715 (Fig. B8 & 7), which were both collected from study area S, most proximal to FHI's carbonatitic

centre (Fig. 3e). The cone sheet sample 519711 exhibits a conspicuous pale spotted texture (Fig. B7a), where pale spots are dominantly feldspath(oidal) (i.e., comprised of much potassic sanidine and more sodic nepheline (cf., Si, K & Na in Fig. B7), while intervening darker areas are predominantly analcimic but also host smaller patches that are less aluminous and distinctly more carbonaceous. As for the alnöite in Figure B5(b), there are fewer augites within these carbonaceous patches, as well as a remarkable abundance of early crystallizing, euhedral perovskites. Although, incompletely mapped, paler 519711's spots are interpreted as incipient sanidine and nepheline crystallization – making the rock phonolitic – while surroundings are dominated by incipient interstitial analcime-carbonate segregations. Otherwise, this sample is also characterized by a greater modal abundance of accessory pyrite than magnetite, while the opposite holds true for the other dyke sample 519715, described further in the main paper (Fig. 7) and supplemented by SEM electron backscatter images and elemental maps in Figure B7.

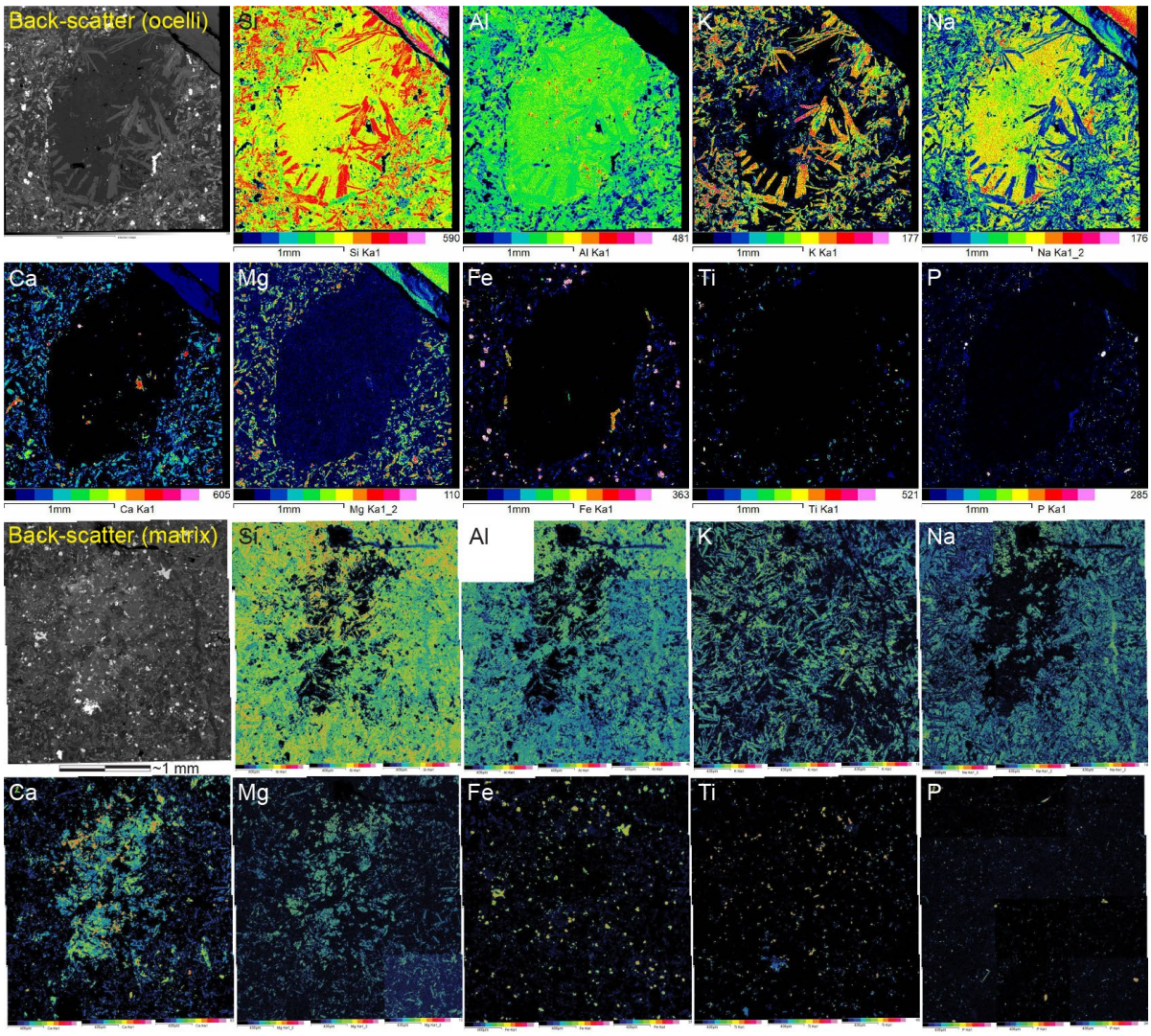

Figure B8: SEM backscatter electronic and elemental maps for both an ocellus (top ten images) and a matrix selection (lower ten images) within the thin section of 519715 (cf., Fig. 7).

B5. Mineral chemistry synthesis

In addition to elemental SEM maps, mainly focusing on ocelli and matrices, SEM spot analyses also determined the mineral chemistry of selected larger crystals within eight thin sections, some of which are described petrographically above and others in the main paper. More specifically, SEM spot analyses were made on phenocrysts and ocelli inside the core of two damtjernitic dykes (Figs. B1 &

4-5), two autolithic nodules (Fig. B4), two carbonaceous alnöites (Figs. B5-6 & 6), as well as a nephelinite sheet (Fig. B7) and dyke (Figs. B8 & 7); i.e., the same samples that are also studied petrographically.

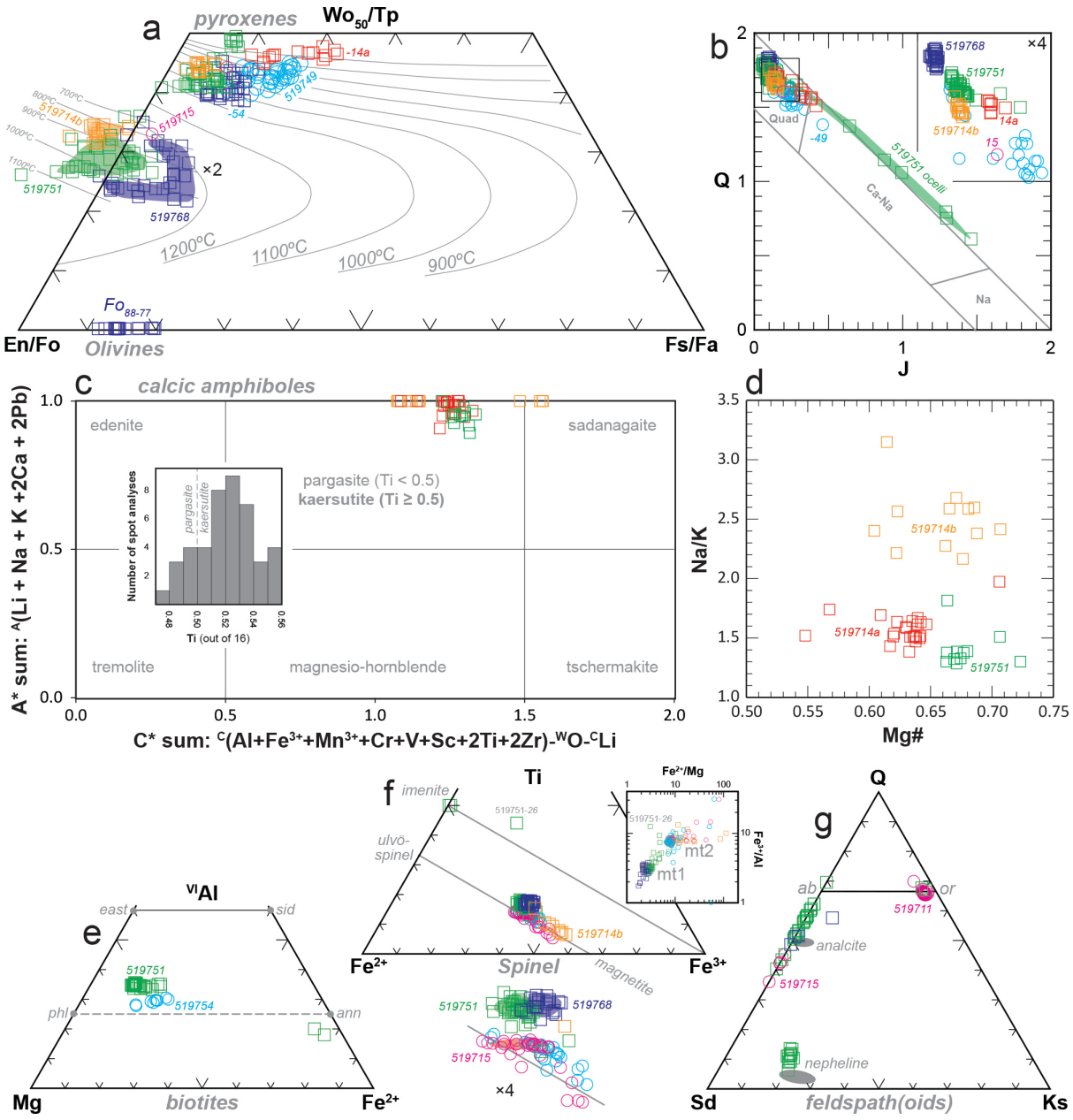

Figure B9: Mineral chemistry (cf., supplementary text A & data D). (a) pyroxene quadrate shows that 519768, -51 & -14b analyses are augites, while 519714a and 519751 ocelli analyses tend to be more sodic (cf., b). 519768 & -51 olivines are also shown along the quadrate's base. (b) Q = Fe^{2+} + Mg + Ca. J = 2 × Na. (c) Amphibole classification according to Locock (2014) shows that most amphiboles are pargasites, where 519714b nodule analyses are slightly more sodic (d). (e) Micas in 519751 plot as Mg-rich biotites, or borderline phlogopite. (f) Spinels are mainly titanomagnetite, where 519751 & -68 tend to have more Mg and Al than 519714b and -15 (insert). (g) Felsic matrix or ocelli minerals are either nephelines, sanidines or scatter around analcime.

The resulting mineral chemistry – listed together with bulk rock geochemistry as Supplementary data D and summarized in Figure B9 – only record slight differences between mafic minerals from the two porphyritic dyke cores and the two nodules, where augites of the most primitive 519768 sample are least alkaline, yet also more Fe-rich (Fig. B9a), and the nodules contain more alkaline augites that grade into becoming aegerines (Fig. B9b). Most amphibole analyses are, according to Locock (2014), more titaniferous kaersutites, grading into a few pargasites (Fig. B9c) and are slightly less magnesian

and more sodic inside the nodules (Fig. B9d). One may argue that micas are sufficiently magnesian to classify as phlogopites, while we prefer to label these as magnesian biotites (Fig. B9e). Opaques are almost exclusively titaniferous magnetite, but where magnetites from porphyritic dyke cores are more magnesian and aluminous (Fig. B9f) than those in both nodules and one more evolved PN-dyke (519715). Finally, the other more evolved nephelinite sheet (519711) comprises of silica-saturated sanidines, while all other samples contain either nepheline or analcime (Fig. B9g).

Reference

LOCOCK, A.J., 2014. An Excel spreadsheet to classify chemical analyses of amphiboles following the IMA 2012 recommendations. *Computers & Geosciences* **62**, 1-11.